NJC

Accepted Manuscript

This is an *Accepted Manuscript*, which has been through the Royal Society of Chemistry peer review process and has been accepted for publication.

Accepted Manuscripts are published online shortly after acceptance, before technical editing, formatting and proof reading. Using this free service, authors can make their results available to the community, in citable form, before we publish the edited article. We will replace this *Accepted Manuscript* with the edited and formatted *Advance Article* as soon as it is available.

You can find more information about *Accepted Manuscripts* in the Information for Authors.

Please note that technical editing may introduce minor changes to the text and/or graphics, which may alter content. The journal's standard Terms & Conditions and the Ethical guidelines still apply. In no event shall the Royal Society of Chemistry be held responsible for any errors or omissions in this *Accepted Manuscript* or any consequences arising from the use of any information it contains.

ROYAL SOCIETY OF CHEMISTRY

www.rsc.org/njc

Cite this: DOI: 10.1039/c0xx00000x

www.rsc.org/xxxxxx

ARTICLE TYPE

Structural, spectroscopic and theoretical studies on dixanthogens: $(ROC(S)S)_2$, with R = n-propyl and isopropyl

Luciana C. Juncal,[a] Yeny A. Tobón,[a‡] Oscar E. Piro,[b] Carlos O. Della Védova[a] and Rosana M. Romano*[a]

Received (in XXX, XXX) XthXXXXXXXXX 20XX, Accepted Xth XXXXXXXXX 20XX

DOI: 10.1039/b000000x

Structural and conformational properties of two dixanthogen molecules, $[CH_3(CH_2)_2OC(S)S]_2$ and $[(CH_3)_2CHOC(S)S]_2$, have been analyzed using a combined experimental and theoretical approach, with data obtained from structural X-ray diffraction methods, IR, Raman and UV-visible spectroscopies, and DFT calculations. $[(CH_3)_2CHOC(S)S]_2$ crystallizes in the monoclinic $P2_1/c$ space group with a=9.735(1), b= 12.588(3), c= 12.131(2) Å, β= 112.65(1)°, and Z=4 molecules per unit cell. The interactions in the crystal were modelled and interpreted by NBO analysis. $[CH_3(CH_2)_2OC(S)S]_2$ is liquid at room temperature, and the vibrational spectra were satisfactorily explained in terms of the equilibrium between three conformers, originated from the rotation of the two terminal CH_3– groups, in agreement with the DFT predictions. The electronic spectra of both dixanthogens were assigned with the assistance of the TD-DFT calculations.

Introduction

Dixanthogens, also known as bisalquilxanthogens, have attracted the attention of chemists since long time ago due to their wide variety of applications, ranging from medicine, industrial uses, and mining.

Dixanthogens, $(ROCSS)_2$, were first prepared in 1824 by Zeise[1] by the mild oxidation of alkali metal xanthates. Even nowadays, the oxidation of xanthates, giving rise to the formation of molecules with a symmetrical disulfide bond, is the most efficient and practical way for the preparation of dixanthogens. Sodium tetrathionate, cyanogen bromide, nitrous acid, and iodine, are some of the oxidizing agents currently used.[2,3,4,5.]

Several studies on the biological activities of this family of compounds have suggested its potential application as antitumoral or antiviral agents, among others. For example, the ability of bisethylxanthogen as inhibitor of carcinogenesis was proposed by different authors[6,7,8] and their use in the treatment of dermatological infections was reported.[9, 10,11] These compounds have also significant commercial applications as regulators to control the polymerization in the manufacture of various synthetic rubbers, resistant to burning and aging.[12,13,14,15]

Although dixanthogens are also used for collectors in froth flotation processes of sulphide minerals,[16,17] the xanthates salts $(ROC(S)S^{-+}M)$ are most widely employed for these applications. However, dixanthogen compounds, proposed as intermediates during the surface interaction between the xanthates and the sulfide minerals, have been suggested as responsible for the flotation process.[18]

$[CH_3(CH_2)_2OC(S)S]_2$, and $[(CH_3)_2CHOC(S)S]_2$ were first synthesized by Whitby and Greenberg by the oxidation of the corresponding potassium xanthate with iodine.[19] The n-propoxy derivative was only characterized by its b.p. (150-5 °C / 0.5 torr)[19] and some IR absorptions.[20] On the other hand, some UV-visible,[21,22] IR[23,24] and NMR[25] spectroscopic studies on the isopropoxy derivative were reported. More recently, this compound has been the subject of Raman studies motivated in the investigation of the surface products produced in the chalcopyrite-sodium isopropylxanthate flotation system, since it is formed on the chalcopyrite surface at high concentration of the collector.[26] However, the reported studies did not provide any indication about the structural properties of these dixanthogen compounds.

In this paper we present a structural and conformational study of two dixanthogen molecules, $(ROC(S)S)_2$, with R = n-propyl and isopropyl, based on single-crystal X-ray diffraction (for the isopropyl derivative) and DFT methods. Results from vibrational (IR and Raman) and electronic (UV-visible) spectroscopies were also interpreted in terms of the molecular conformations and structures.

Methodology

Synthesis

Reagents and solvents were purchased reagent grade and used without further purification. Xanthate salts, $ROC(S)S^{-+}K$, were produced from KOH, CS_2, and the corresponding alcohol, ROH.[27] $[ROC(S)S]_2$, R = $CH_3(CH_2)_2$– and $(CH_3)_2CH$–, were synthesized by the oxidation of $ROC(S)S^{-+}K$ with I_2, according to the technique reported in the literature.[19] $[CH_3(CH_2)_2OC(S)S]_2$ was obtained as a yellow oil and purified by successive extractions using diethyl ether. $[(CH_3)_2CHOC(S)S]_2$, a white crystalline solid, was purified by successive crystallizations using isopropyl alcohol at 45 ºC. The final purity of both compounds

was checked by GC-MS and NMR (^{1}H, ^{13}C).

X-ray diffraction analysis

Single crystal X-ray diffraction data of $[(CH_3)_2CHOC(S)S]_2$ were collected on an Enraf-Nonius CAD4 diffractometer at 296 K (graphite monochromatic CuKα radiation, λ = 1.54184 Å) with the program EXPRESS[28] and reduced with XCAD4.[29] The unit cell parameters were obtained by least-squares refinement (based on the angular setting of 25 reflections in the θ-range from 18.45 to 87.14º) using EXPRESS. The data were corrected for absorption with PLATON.[30] The structure was solved by direct methods with the program SHELXS of the SHELX package[31] and the corresponding molecular models developed by alternated cycles of Fourier methods and full-matrix least-squares refinement on F^2 with SHELXL of the same suite of programs. The hydrogen atoms were positioned stereo-chemically and refined with the riding model. The methyl H-positions were optimized by treating them as rigid groups which were allowed to rotate during the refinement around the corresponding C-C bonds such as to maximize the residual electron density at the calculated positions. As a result, all CH_3 groups converged to staggered conformations. Crystallographic structural data are presented as Supplementary Material (Tables S1-S6).

FTIR spectroscopy

The FTIR spectra were recorded on a Nexus Nicolet instrument equipped with either an MCTB or a DTGS detector (for the ranges 4000–400 cm^{-1} or 600–100 cm^{-1}, respectively) at room temperature and with a resolution of 4 cm^{-1}. The solid compound was measured in KBr (range 4000-400 cm^{-1}), CsI (range 600-180 cm^{-1}) and polyethylene (range 600-100 cm^{-1}) pellets, while the spectra of the liquid compound were measured using KBr, CsI and polyethylene windows, to cover the range between 4000 and 100 cm^{-1}.

FTRaman spectroscopy

The FTRaman spectra were measured in a Bruker IFS 66 FTRaman spectrometer, using a resolution of 4 cm^{-1}, in the region between 3500 and 100 cm^{-1}. The samples, placed in a sealed 2 mm glass capillary, were excited with a 1064 nm Nd-YAG laser. The resonance or pre-resonance Raman effect was discard, after the investigation of both samples using an Horiba-Jobin-Yvon T64000 Raman spectrometer, with a confocal microscope and CCD detection, when excitation light of Ar and Kr multilines lasers was used.

NMR spectroscopy

The ^{1}H (200 MHz) and ^{13}C (50 MHz) NMR spectra of $[CH_3(CH_2)_2OC(S)S]_2$ were measured at 298 K on a Varian Mercury Plus 200 spectrometer. The sample was dissolved in $CDCl_3$ in a 5 mm NMR tube. Chemical shifts, δ, are given in ppm relative to TMS (δ = 0 ppm). The ^{1}H NMR spectrum presents a triplet at 0.98 ppm (J = 7.3 Hz), a multiplet between 1.73-1.91 ppm, and a triplet at 4.55 ppm (J = 6.3 Hz) that correspond to the hydrogen atoms of the CH_3–, –CH_2– and –CH_2O– groups, respectively. The $^{13}C\{^1H\}$ NMR spectrum shows four signals at 10.7, 21.8, 76.7 and 207.6 ppm assigned to CH_3–, –CH_2–, –CH_2O– and –C(S)S–, respectively. The spectra are shown in Figs. S1 and S2 of the Supporting Information, while a comparison with related molecules are presented in Tables S7 and S8.

Gas chromatography - mass spectrometry

The GC-MS analysis of both samples was carried out on a Shimadzu QP-2010. Details are given in Table S9 of the Supplementary Material. Only one peak was observed in the chromatograms of either $[CH_3(CH_2)_2OC(S)S]_2$ or $[(CH_3)_2CHOC(S)S]_2$, with t_R = 10.0 and 13.5 min., respectively, denoting the purity of the samples. The complete mass spectra of the compounds are presented as Supplementary Material (Fig. S3 and Table S10). Following electron impact ionization (70 eV, ion source temperature = 200 °C) of the n-propyl derivative $C_3H_7^+$ (m/z=43), $C_3H_5^+$ (m/z=41), and $C_2H_3^+$ (m/z=27) were found to be the most abundant fragments. The molecular ion M^+ (m/z=270) was also detected with an abundance below 1%. The mass spectrum of $[(CH_3)_2CHOC(S)S]_2$ taken at the same experimental conditions shows the fragments $(CH_3)_2CH^+$ (m/z=43), $C_3H_5^+$ (m/z=41), $SSC(S)^+$ (m/z=108), $C_2H_3^+$ (m/z=27), $OC(S)SSC(S)^+$ (m/z=168), and SCS^+ (m/z=76), beside the M^+ peak at m/z=270.

UV-visible spectroscopy

UV-vis spectra in the 200-800 nm range of solutions of both samples in solvents of different polarity were recorded at room temperature on a Hewlett Packard UV-VIS spectrometer using a 1 cm-quartz cell.

Theoretical calculations

All of the quantum chemical calculations were performed using the Gaussian 03 program system,[32] using the B3LYP method in combination with a 6-31+G* basis set. Geometry optimizations were sought using standard gradient techniques by simultaneous relaxation of all the geometrical parameters. The calculated vibrational properties correspond in all cases to potential energy minima for which no imaginary vibrational frequency was found. The electronic spectra were simulated using the TD-DFT formalisms over the previously optimized structures, with a maximum of 100 states and S=1.[33,34]

Results and discussion

Structural theoretical calculations

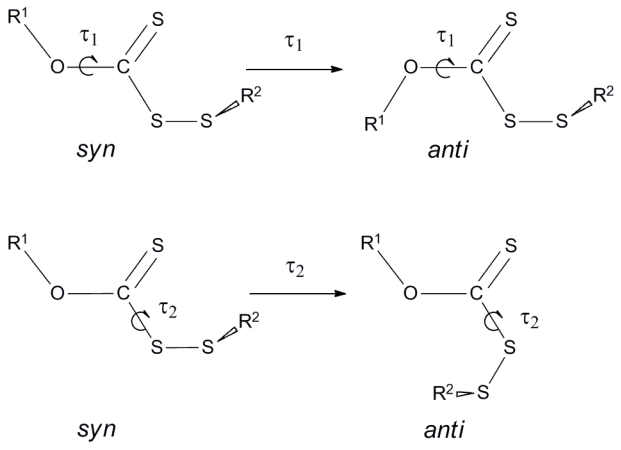

Scheme 1 Schematic representation of the *syn* and *anti* orientation in terms of the dihedral angles τ_1 and τ_2.

Molecules having the framework $R^1OC(S)S-$ can, in principle, adopt different conformations through internal rotation around either the C–O (τ_1) or C–S (τ_2) single bonds (see Scheme 1). Previous structural studies on molecules containing the –OC(S)S– moiety reported by our group show that the most stable conformation is *syn-anti* (*syn* with respect to the C–O single bond and *anti* with respect to the C-S single bond).[35,36] On the other hand, it is well known that the *gauche* conformation is adopted around a disulphide single bond.[37]

For the n-propyl dixanthogen, $[CH_3(CH_2)_2OC(S)S]_2$, besides the torsional angles around each of the C–O and C–S single bonds, the values of two other torsions related with each of the propoxy groups, i.e. τ(CCOC) and τ(CCCO), are necessary to describe the conformational properties of the molecule. Taking into account all possible conformations as starting structures, eleven forms were found as energy minima, for which no imaginary frequencies occur, when the B3LYP/6-31+G* approximation was employed for the calculations. The molecular models of the conformers of $[CH_3(CH_2)_2OC(S)S]_2$ are shown in Fig. S4, while the relevant dihedral angles and predicted relative energy differences (corrected by zero-point energy) are presented in Table S11. The different conformers can be associated into three groups, according to their energy differences, being the relevant parameter for this classification the value adopted by the torsional angle around each of the C–S single bonds. In the first group, composed by structures I-III depicted in Fig. 1, both C–S torsional angles are close to 180°, denoting by **A** (*anti*) in the figure. The differences between these three structures are the conformations adopted by the terminal CH_3 groups, which may be *anti* or *gauche* with respect to the C–O single bond. Structure I, with both terminal methyl groups in *anti* orientation, is predicted to be the more stable one. Structure II, which maintain one terminal methyl group *anti* while the second is in *gauche* position, is predicted only 0.08 kcal mol^{-1} higher in energy. Structure III, with an energy difference of 0.26 kcal mol^{-1} from structure I, possesses both terminal methyl groups in *gauche* orientation.

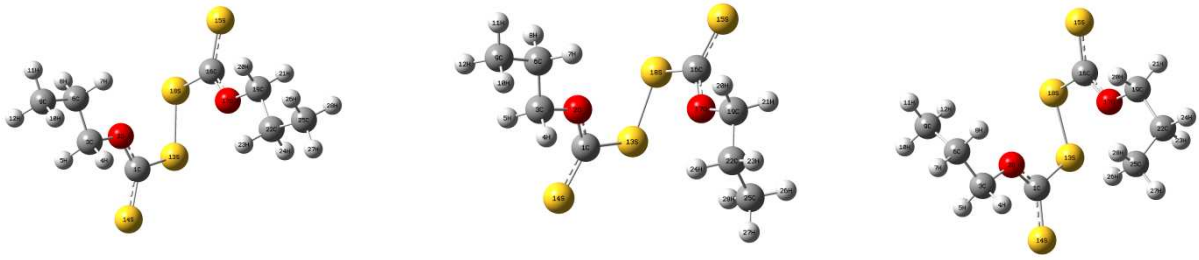

I II III

Fig 1 Molecular models of the three most stable conformers of $[CH_3(CH_2)_2OC(S)S]_2$ calculated with the B3LYP/6-31+G* approximation.

The second group formed by structures IV-VIII, with energy differences between 1.5-1.8 kcal/mol with respect to the most stable form (structure I), possess one C-S torsional angle close to *anti* conformation and the other close to *syn*. As in the first group, in this case the differences in the structures arise also from the orientation adopted by the terminal methyl groups. In the last three structures (IX-XI), with computed energy differences between 2.8 and 3.0 kcal/mol with respect to the form I, both C-S torsions are close to *syn* conformation. All the structures depicted in Fig. S4 and listed in Table S11 present the C–C–O–C torsional angles close to 180° (*anti*) and the C–O–C=S angles close to 0° (*syn*).

The theoretical conformational study of the isopropyl derivative was simpler than that of the n-propyl dixanthogen, due to the reduced number of torsional angles in the molecule. Table S12 of the Supplementary Information presents the values of the relevant dihedral angles and relative energy differences (corrected by zero-point energy) for the forms founded as the most stable structures of $[(CH_3)_2CHOC(S)S]_2$, according to the B3LYP/6-31+G* approximation (see Fig. S5). As in the case of the n-propyl derivative, the structures differ only in the value of the torsion around the C–S single bonds. The stability order, as well as the energy differences, is also in agreement with the structures predicted for the molecule described previously. In the most stable form (I) the conformation around both C–S single bonds are close to *anti*. The second conformer (II), about 1.6 kcal/mol higher in energy, presents one C–S torsion close to *anti* while the other one is almost *syn*, and the third form (III), with an energy difference of 2.9 kcal/mol with respect to the most stable one, presents both dihedral angles around the C-S bonds close to 0°. The molecular models of the three stable structures of $[(CH_3)_2CHOC(S)S]_2$ are presented in Fig. S5 of the Supplementary Information. As in the case of $[CH_3(CH_2)_2OC(S)S]_2$, all the structures present C–O–C=S dihedral angles close to 0° (*syn*).

The calculated dipole moments and net atomic charges obtained by Mulliken population analysis for the most stable structures of both disulphides are presented in Table S13 of the Supplementary Information.

Crystal structure

Bis[isopropoxy(thiocarbonyl)]disulfane, $[(CH_3)_2CHOC(S)S]_2$, crystallizes in the monoclinic $P2_1/c$ space group with a = 9.735(1), b = 12.588(3), c = 12.131(2)Å, β = 112.65(1)°, and Z=4 molecules per unit cell. The $[(CH_3)_2CHOC(S)S]_2$ consists of two un-equivalent $(CH_3)_2CHOC(S)S$ groups linked by a S–S single bond [d(S-S)=2.042(2) Å]. The dihedral C–S–S–C angle is 85.0 (2)°. For full crystallographic data and refinement information, see Supporting Information.

The molecule $[(CH_3)_2CHOC(S)S]_2$ is at a general crystal

position and only the conformation *syn-anti-gauche-anti-syn* is observed in a single crystal at 296(2) K, in coincidence with the prediction of the quantum chemical calculations for the most stable form of the isolated molecule. Fig. 2 shows an ORTEP[38] plot of the molecule. Selected geometrical parameters are listed in Table 1 where they are compared with the corresponding ones calculated with DFT methods for the theoretically most stable conformer.

If compared with bis[ethyl(thiocarbonyl)]disulfane,[39] the S–S distance of $[(CH_3)_2CHOC(S)S]_2$ is slightly shorter: 2.042(2) and 2.054(4) Å for the isopropyl and ethyl dixanthogens, respectively. The disulphide dihedral angle is also smaller in the isopropyl derivative, 85.0(2)°, than in the ethyl compound, 107.2(1)°.**¡Error! Marcador no definido.**

The crystal packing of the molecules, shown in Fig. 3, consists of zig-zag chains of molecules held together by 2.946 Å –C=S···H interactions, 0.05 Å shorter than the sum of the van der Waals radii.[40] Each disulphide molecule interacts through a sulphur atom of one of the thiocarbonylic group with a hydrogen of a methyl group of another molecule, and also through one of the terminal hydrogen atom with a S of a third molecule, forming endless zig-zag chains (schematized in light-blue in Fig. 3). The crystal framework is completed through a second type of interaction: sulphur–sulphur contacts that held a couple of enantiomeric molecules together at a distance of 3.719 Å (schematized in green in Fig. 3).

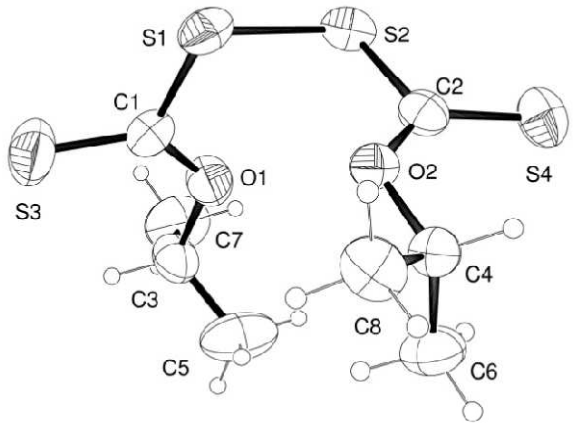

Fig. 2 Drawing of the solid state $[(CH_3)_2CHOC(S)S]_2$ molecule showing the labeling of the non-H atoms and their displacement ellipsoids at the 30% probability level.

Table 1 Selected experimental (X-ray diffraction) and calculated (for the structure I with B3LYP/6-31+G*) bond distances (r [Å]) and angles (α and τ [°]) of $[(CH_3)_2CHOC(S)S]_2$

Geometrical parameters	X-ray diffraction	B3LYP/6-31+G*
r [C(8)–C(4)]	1.487(6)	1.521
r [C(6)–C(4)]	1.504(5)	1.523
r [O(2)–C(4)]	1.478(4)	1.476
r [C(2)–O(2)]	1.291(4)	1.318
r [C(2)–S(4)]	1.635(4)	1.651
r [S(2)–C(2)]	1.767(4)	1.786
r [S(1)–S(2)]	2.042(2)	2.110
r [C(1)–S(1)]	1.758(4)	1.786
r [S(3)–C(1)]	1.619(4)	1.651
r [O(1)–C(1)]	1.298(4)	1.318
r [C(3)–O(1)]	1.488(5)	1.476
r [C(5)–C(3)]	1.475(8)	1.523
r [C(7)–C(3)]	1.493(8)	1.521
α [O(2)–C(4)–C(6)]	107.8(3)	108.48
α [C(2)–O(2)–C(4)]	119.3(3)	121.30
α [O(2)–C(2)–S(4)]	130.3(3)	129.51
α [O(2)–C(2)–S(2)]	114.4(3)	114.02
α [C(2)–S(2)–S(1)]	106.0(1)	107.34
α [C(1)–S(1)–S(2)]	106.1(1)	107.34
α [S(1)–C(1)–S(3)]	116.1(2)	116.47
α [S(1)–C(1)–O(1)]	114.5(3)	114.02
α [C(1)–O(1)–C(3)]	120.9(3)	121.30
α [O(1)–C(3)–C(5)]	106.3(4)	108.48
α [O(1)–C(3)–C(7)]	113.4(5)	105.49
τ [C(2)–O(2)–C(4)–C(8)]	152.5(3)	148.6
τ [C(2)–O(2)–C(4)–C(6)]	–85.7(4)	–88.9
τ [C(4)–O(2)–C(2)–S(4)	0.1(5)	–3.1
τ (S(1)–S(2)–C(2)–S(4)]	–176.4(2)	178.1
τ [C(1)–S(1)–S(2)–C(2)]	–85.0(2)	–86.2
τ [S(2)–S(1)–C(1)–S(3)]	–178.4(2)	178.1
τ [C(3)–O(1)–C(1)–S(3)]	2.3(6)	–3.1
τ [C(1)–O(1)–C(3)–C(5)]	–128.8(5)	–88.9
τ [C(1)–O(1)–C(3)–C(7)]	109.8(5)	148.6

To help in the interpretation of the interactions present in the crystal packing, the charge transfer and also the electrostatic interactions were studied using theoretical approximations. The former type of interactions was modelled including 12 molecules and with the help of Natural Bond Orbital (NBO) analysis[41,42] at the B3LYP/6-31+G* level of approximation. Table 2 presents some significant donor-acceptor orbital interactions for the C=S···H–C and C=S···S–C contacts and their second-order perturbation stabilization energies (ΔE_2), the energy difference between the interacting orbitals E(j)-E(i) and the value of Fock´s integral F(i,j). Fig. 4 shows the orbital interaction picture of the most important contributions (for clarity purposes only three molecules were depicted to show each type of interaction).

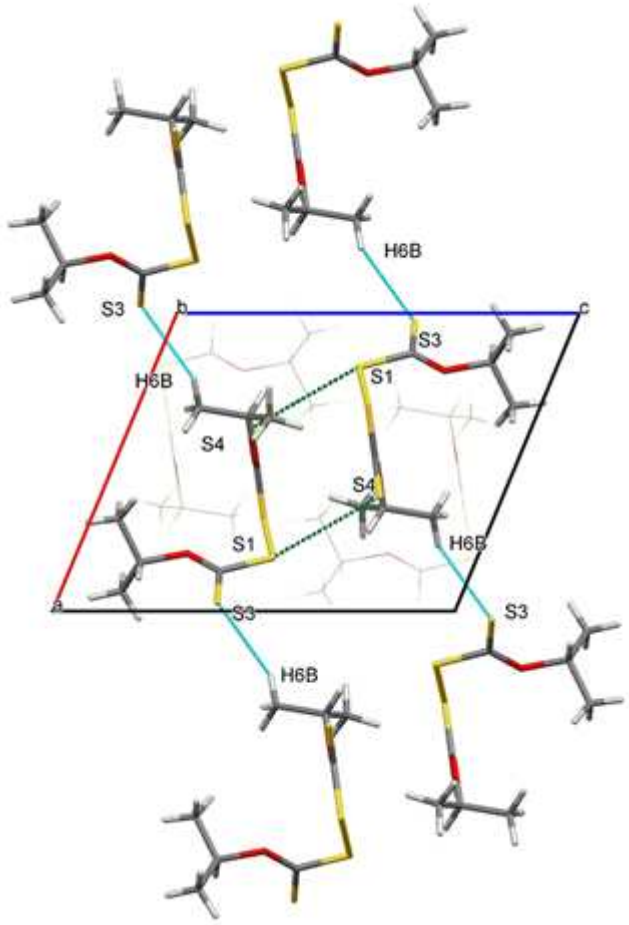

Fig. 3 Crystal packing of $[(CH_3)_2CHOC(S)S]_2$ obtained by X-Ray crystallography.

Vibrational study

Figs. 5 and 6 depict the experimental IR and Raman spectra of both dixanthogen molecules. A complete list of the wavenumbers is presented as Supplementary Material (Tables S14 and S15). Although some bands of the IR spectra of $[(CH_3)_2CHOC(S)S]_2$[23,24] and $[CH_3(CH_2)_2OC(S)S]_2$[20] were previously reported in the literature, a complete vibrational analysis was not yet published.

The IR and Raman spectra of $[CH_3(CH_2)_2OC(S)S]_2$ can be clearly interpreted in terms of the conformational equilibrium previously discussed in this paper. The most intense absorption in the experimental IR spectrum of $[CH_3(CH_2)_2OC(S)S]_2$ occurs at 1018 cm^{-1}, with shoulders at 1036 and 1049 cm^{-1}. The first two bands are assigned to the ν C=S *out-of-phase* and *in-phase* vibrational modes, respectively. According to the B3LYP/6-31+G* approximation, these vibrations are predicted at 1042/1060, 1036/1055 and 1032/1047 cm^{-1}, for structures I, II and III respectively, with the *out-of-phase* mode more than three times more intense than the *in-phase* vibration. In this spectral region two other less-intense absorptions of conformer III and one of conformer II are also expected, arising from the ν_{as} C–C–C modes (see Tables S14), that can be correlated with the 1049 cm^{-1} band.

Table 2 Donor-acceptor orbital interactions for the C=S···S–C and the C=S···H–C contacts of $[(CH_3)_2CHOC(S)S]_2$ and their second-order perturbation stabilization energies (ΔE_2, kcal.mol^{-1}), the energy difference between the interacting orbitals E(j)-E(i)) and the value of Fock´s integral F(i,j), both in atomic units (a.u.), calculated with the B3LYP/6-31+G* approximation (atom numbering is presented in Figure 4)

Donor NBO (i)	Acceptor NBO (j)	E(2) kcal/mol	E(j)-E(i) a.u.	F(i,j) a.u.
C=S(31)···S(1)–C				
from unit 1 to unit 2				
LP_x S(1)	π* S(31)– C(35)	0.10	0.66	0.008
LP_y S(1)	π* S(31)– C(35)	0.11	0.26	0.005
from unit 2 to unit 1				
π S(31)=C(35)	σ* S(1)–C(6)	0.24	0.57	0.011
LP_y S(31)	σ* S(1)–C(6)	0.10	0.37	0.006
C=S(3)···S(28)–C				
from unit 1 to unit 2				
π S(3)=C(7)	σ* S(28)–C(34)	0.23	0.58	0.010
LP_x S(3)	σ* S(28)–C(34)	0.10	0.38	0.006
from unit 2 to unit 1				
LP S(28)	π* S(3)– C(7)	0.11	0.67	0.008
LP S(28)	π* S(3)–C (7)	0.11	0.26	0.005
C=S(4)···H(74)–C(72)				
from unit 1 to unit 3				
LP_x S(4)	σ* C(72)–H(74)	0.65	1.42	0.027
LP_y S(4)	σ* C(72)–H(74)	0.94	0.90	0.027
σ C(6)=S(4)	σ* C(72)–H(74)	0.08	1.03	0.008
π C(6)=S(4)	RY* H(74)	0.13	1.55	0.013
LP_z S(4)	RY* H(74)	0.08	1.53	0.010
from unit 3 to unit 1				
σ C(72)–H(74)	π*C(6)=S(4)	0.10	0.81	0.008

σ* S(1)–C(6)

The second intense feature in the IR spectrum of Fig. 5 appears at 1266 cm^{-1}, and can be assigned to the unresolved *out-of-phase* and *in-phase* ν C–O modes (corresponding to the O–C(S)– group). Theoretical calculations predict a small wavenumber difference for these two vibrational modes, and also almost no difference between the three conformers (1292/1297, 1292/1298 and 1293/1298 cm^{-1}, for structures I, II and II, respectively), which is in accordance with the experimental observation.

The most intense bands of the Raman spectrum of $[CH_3(CH_2)_2OC(S)S]_2$ correspond to the C–H stretching modes of the n-propyl groups. In the low energy region, the 498 cm^{-1} band can be associated with the ν S–S mode, characteristic of disulphide molecules. For the most stable conformer this mode is predicted as the most intense one for this spectral region, at 444 cm^{-1}. In forms II and III, the theoretical ν S–S vibrations are at 461 and 471 cm^{-1}, respectively. In both cases this mode is predicted with lower intensity than in form I, but accompanied by two other modes with comparable intensities, at 419 and 442 cm^{-1} (for structure II) and 413 and 442 cm^{-1} (for structure III), that explain the complex pattern observed in the experimental Raman spectrum (for more detail see Table S14 of the Supplementary Information). The Raman band at 1036 cm^{-1}, assigned to the ν C=S *in-phase* vibrational mode of structure I, present a shoulder at 1018 cm^{-1}, that can be attributed to the ν C=S *out-of-phase*

modes of the three conformers and also to the ν_{as} C–C–C of forms I. A complete list of the IR and Raman experimental bands of $[CH_3(CH_2)_2OC(S)S]_2$ and proposed assignment is presented in Table S14.

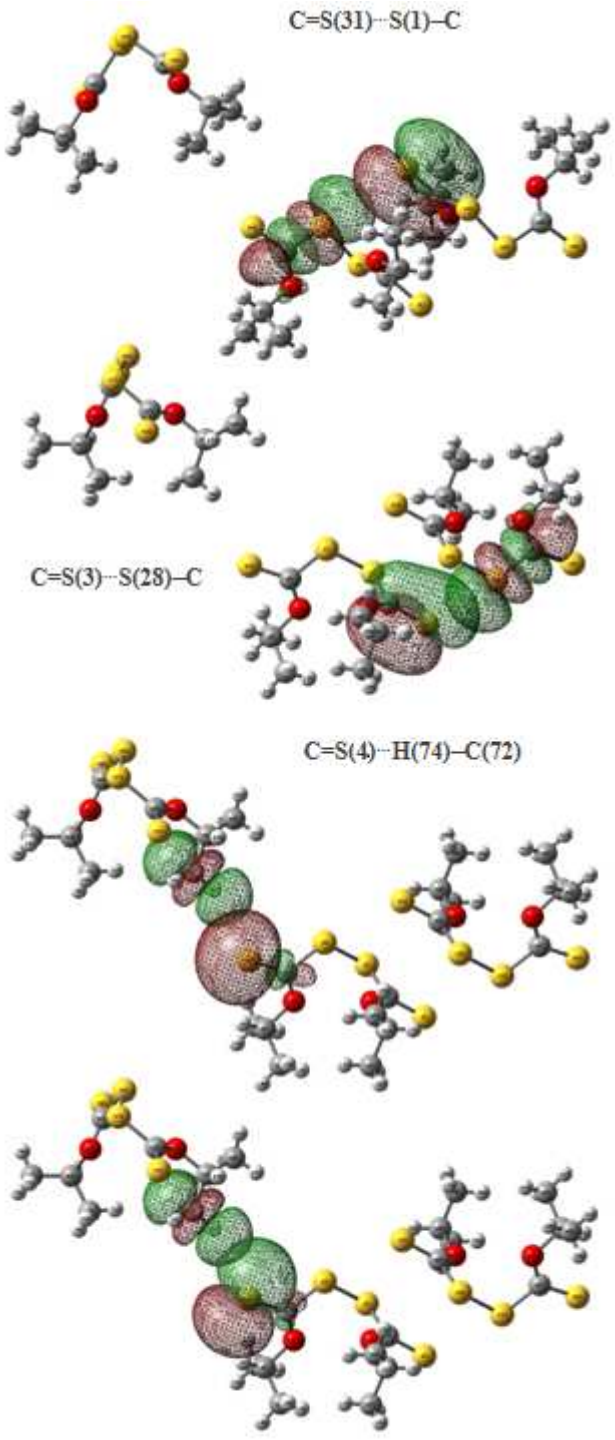

Fig. 4 NBO interaction picture of the most important contributions observed in the crystal packing of $[(CH_3)_2CHOC(S)S]_2$ calculated with the B3LYP/6-31+G* approximation.

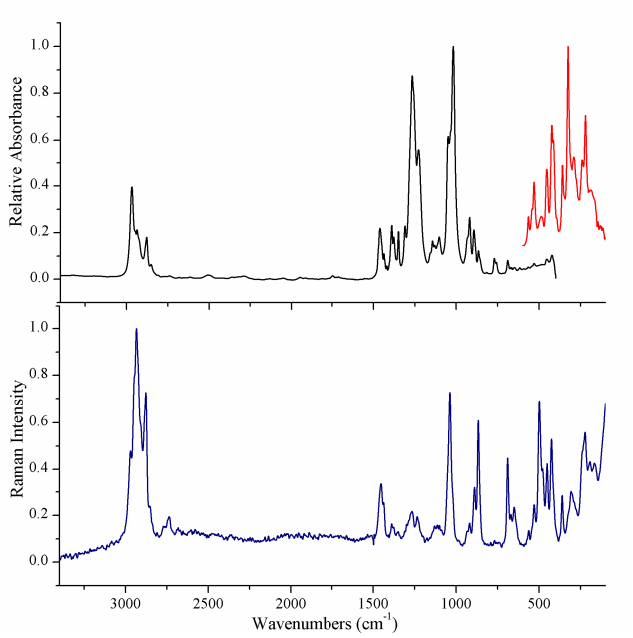

Fig. 5 IR (black trace between 3500–400 cm^{-1} and red trace between 600–100 cm^{-1}) and Raman (lower blue trace, between 3500–100 cm^{-1}) spectra of liquid $[CH_3(CH_2)_2OC(S)S]_2$.

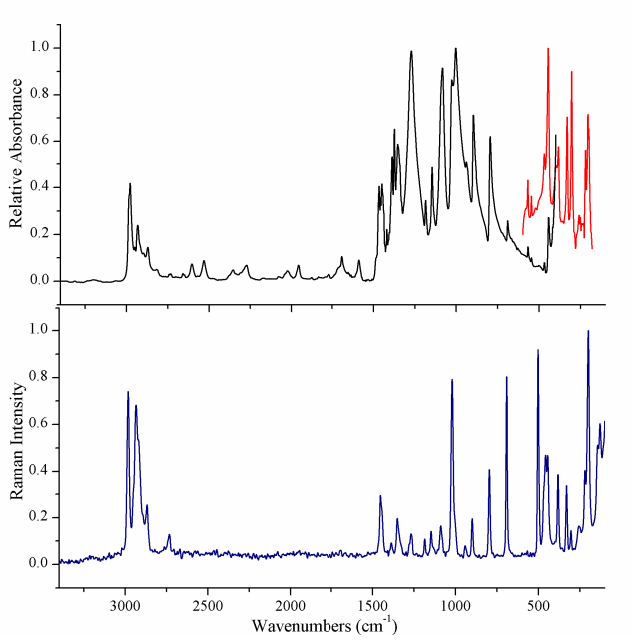

Fig. 6 IR (black trace between 3500–400 cm^{-1} and red trace between 600–180 cm^{-1}) and Raman (lower blue trace, between 3500–100 cm^{-1}) spectra of solid $[(CH_3)_2CHOC(S)S]_2$.

On the other hand, the vibrational spectra of $[(CH_3)_2CHOC(S)S]_2$ shown in Fig. 6 can be completely explained in terms of the only one conformer found in the crystal. The molecule belongs to the C_2 symmetry point group, with their 78 normal modes of vibration active in both IR and Raman, classified as 40A + 38B. Table S15 of the Supplementary Information compiles all vibrational wavenumbers, together with the proposed assignment.

Table 3 IR and Raman wavenumbers of both disulphides assigned to the nine stretching modes of the ROC(S)SSC(S)OR moiety

$[CH_3(CH_2)_2OC(S)S]_2$			$[(CH_3)_2CHOC(S)S]_2$			Assignment
Experimental		B3LYP/	Experimental		B3LYP/	
IR	Raman	6-31+G*	IR	Raman	6-31+G*	
1283	1298	1297	-	1278	1306	ν_{C-O} *i.p.*
1266	1265	1292	1272	1268	1301	ν_{C-O} *o.f.p.*
1036	1036	1060	1027	1019	1032	$\nu_{C=S}$ *i.p.*
1018	1018	1042	1004	1002	1016	$\nu_{C=S}$ *o.f.p.*
920	918	952	795	-	806	ν_{O-R} *o.f.p.*
		902	-	795	804	ν_{O-R} *i.p.*
690	688	699	690	-	694	ν_{C-S} *o.f.p.*
-	670	699	-	691	693	ν_{C-S} *i.p.*
	498	444	-	501	478	ν_{S-S}

Table 3 presents only the IR and Raman wavenumbers of both disulphides assigned to the nine stretching modes of the ROC(S)SSC(S)OR moiety, together with the predicted ones by the B3LYP/6-31+G* approximation. It is worth to mention the wavenumber differences of more than 300 cm^{-1} between ν C–O and ν O–R normal modes, indicative of a π delocalization of the C=S doble bond through the adjacent C–O single bond. This assignment is in accordance with the X-ray diffraction values of 1.291 and 1.478 Å for the C–O and O–R distances, respectively, for $[(CH_3)_2CHOC(S)S]_2$ (see Table 1). It is also interesting to note that the wavenumbers of the vibrational stretching modes of the ROC(S)SSC(S)OR moiety are very similar for both dixanthogens, with the only exception of the bands assigned to the ν O–R normal modes, that appear at lower wavenumber in the isopropyl derivative, indicating longer O–R distances in this molecule with respect to same distances in the n-propyl species. These differences can be interpreted in terms of steric effects, relevant for R = isopropyl.

Electronic absorption spectroscopy

The UV-visible spectra of both disulphides in solution of different solvents were measured. Table 4 compiles the wavelength of the absorption maxima of the spectra together with the extinction coefficients. The spectra are characterized by three bands, presenting a forth absorption in some solvents, as can be observed in the table.

To help in the interpretation of the electronic spectra, TD-DFT calculations were performed. Tables S16 and S17 list the wavelength and oscillator strength of the predicted monoelectronic transitions for both dixanthogens, while Figs. S6 and S7 depict the calculated electronic spectra. As the simulated spectra are very similar for the three most stable conformers of $[CH_3(CH_2)_2OC(S)S]_2$, the presented results correspond only to structure I. Comparison between experimental and calculated electronic spectra, and the calculated molecular orbitals relevant for the electronic transitions, are presented in Figs. 7 and 8.

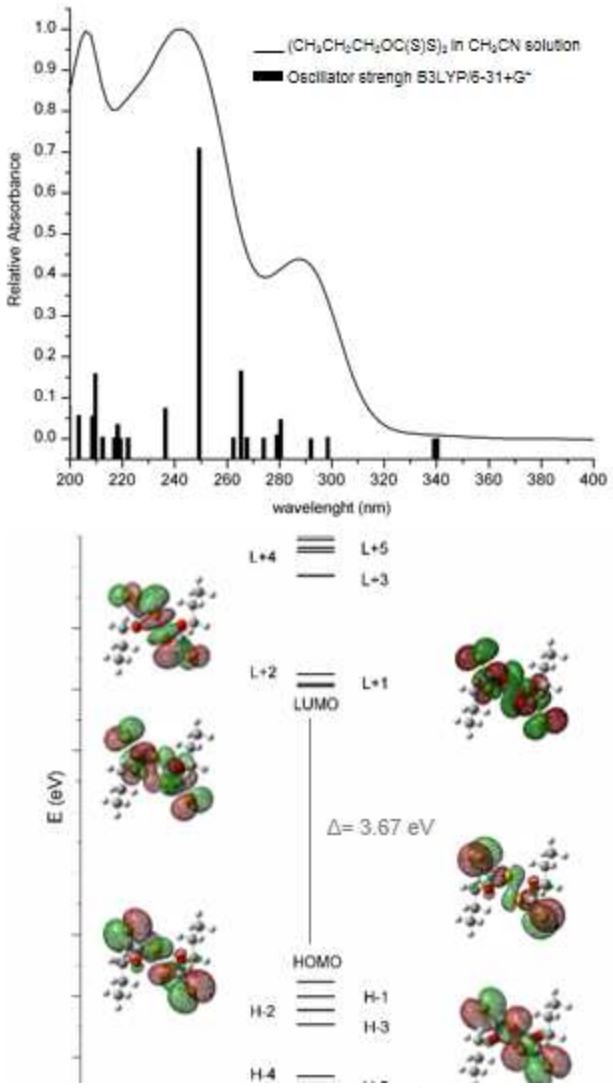

Fig. 7 Experimental UV spectrum (in CH_3CN, full trace), calculated oscillator strength of the electronic transitions (B3LYP/6-31+g(d), black bars) and schematic representation of the molecular orbitals involved in the most intense electronic transitions of $[CH_3(CH_2)_2OC(S)S]_2$. The energy scale is only qualitative.

Table 4. Absorption maxima (nm) of the UV spectra of both disulphides in solution of different solvents. Extinction coefficients (ε, $Lmol^{-1}cm^{-1}$) are given between parentheses

	$[CH_3(CH_2)_2OC(S)S]_2$			Assignment
CH_3CN	$CH_3(CH_2)_2OH$	$CHCl_3$	CCl_4	
206 (18000)				
242 (19100)	244 (11820)			$n\rightarrow\sigma^*_{C=S}$
288 (7690)	286 (4830)	290 (4900)	288 (9500)	$\pi\rightarrow\pi^*_{OC(S)S}$
354 (80)	358 (40)	356 (105)	360 (100)	$n\rightarrow\pi^*_{OC(S)S}$
	$[(CH_3)_2CHOC(S)S]_2$			
H_2O	$(CH_3)_2CHOH$	CCl_4		
226	226 (15690)			$n\rightarrow\sigma^*_{C=S}$
258	242 (17060)			$n\rightarrow\sigma^*_{C=S}$
300	286 (8250)			$\pi\rightarrow\pi^*_{OC(S)S}$
	360 (60)	362 (80)		$n\rightarrow\pi^*_{OC(S)S}$

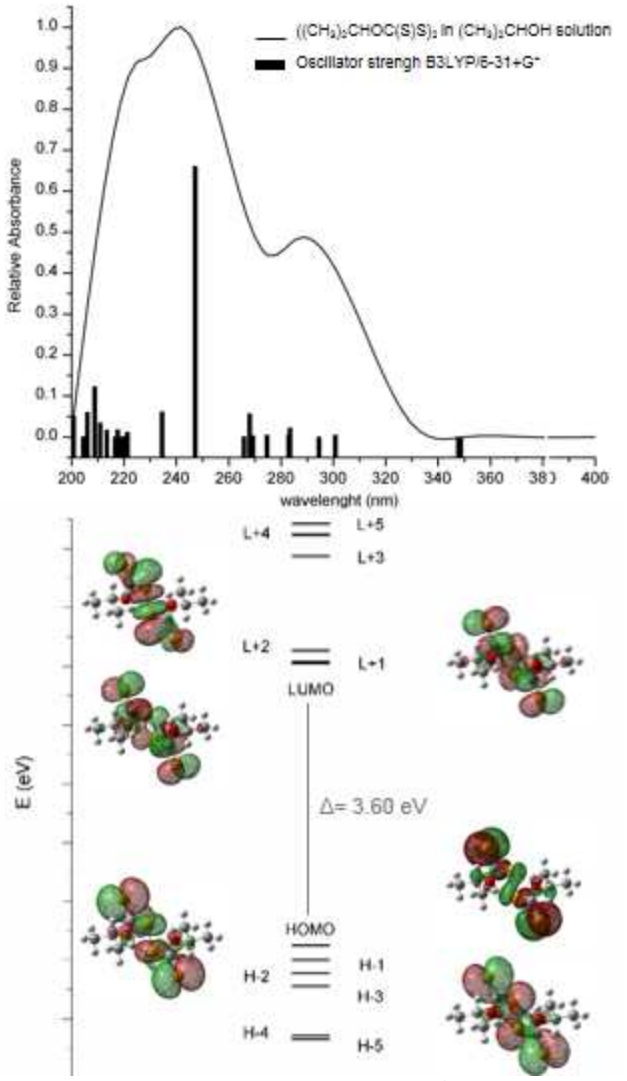

Fig. 8 Experimental UV spectrum (in $(CH_3)_2CHOH$, full trace), calculated oscillator strength of the electronic transitions (B3LYP/6-31+g(d), black bars) and schematic representation of the molecular orbitals involved in the most intense electronic transitions of $[(CH_3)_2CHOC(S)S]_2$. The energy scale is only qualitative.

As can be observed in Figs. 7 and 8 and in Table 4, the UV spectra of both molecules are very similar, related with the fact that the electronic transitions responsible for the absorptions are mostly related with the –OC(S)S– groups, which are, at least by the evidence of the vibrational spectra, almost independent of the R substituent.

Conclusions

The most remarkable difference between the two title molecules is their aggregation state at ambient temperatures. While $[(CH_3)_2CHOC(S)S]_2$ is solid, $[CH_3(CH_2)_2OC(S)S]_2$ is a liquid, with a melting point difference greater than 40 °C. One possible explanation for this distinctive behaviour could be the conformational flexibility of the n-propyl derivative. As discussed previously, three different conformers with very low energy differences are expected for $[CH_3(CH_2)_2OC(S)S]_2$, according to the orientation adopted by the terminal CH_3 groups. On the other hand, theoretical calculation predict only one conformer for $[(CH_3)_2CHOC(S)S]_2$, in agreement with the structure determined by X-ray diffraction. Other factors can contribute to the differences in the melting point of related analogous compounds. One of them can be attributed to the arrangement capabilities of the molecules, according to their shape and electrostatic potential (see for example refs. 43 and 44). However, this does not seem to be the reason for the observed difference, since the calculated electrostatic potentials and molecular shapes are not very different for both compounds, as well as the stabilization for intermolecular interactions.

A detailed analysis of the vibrational (IR and Raman) spectra, with the assistance of the results of DFT calculations, is also consistent with the conformational study. While the spectra of $[(CH_3)_2CHOC(S)S]_2$ were completely explained in terms of one form, for the assignment of all the observed bands in the IR and Raman spectra of $[CH_3(CH_2)_2OC(S)S]_2$ the contribution of the three conformers were necessary. The UV-visible spectra of both molecules are very similar, and independent of the conformation for the n-propyl derivative, due to the fact that the electronic transitions are mostly related with the –OC(S)S– moieties.

Acknowledgments

C.O.D.V. and R.M.R. thank the Consejo Nacional de Investigaciones Científicas y Técnicas (CONICET) (PIP 4695), the Comisión de Investigaciones Científicas de la Provincia de Buenos Aires (CIC), the Agencia Nacional Científica y Tecnológica (PICT 33878) and the Facultad de Ciencias Exactas, Universidad Nacional de La Plata, for financial support. RMR is also grateful to the Fundación Antorchas. In addition, Y.A.T. acknowledges with thanks a Deutscher Akademischer Austausch Dienst (DAAD) award. CODV especially acknowledges the DAAD, which generously sponsors the DAAD Regional Program of Chemistry of the Republic Argentina supporting Latin-American PhD students in La Plata. O.E.P is a Research Fellow of CONICET. The X-ray diffraction data were collected at LANADI (CONICET).

Notes and references

[a] *CEQUINOR (CONICET-UNLP), Departamento de Química, Facultad de Ciencias Exactas, Universidad Nacional de La Plata, 47 esq. 115, (1900) La Plata, Argentina. E-mail: romano@quimica.unlp.edu.ar*
[b] *Departamento de Física, Facultad de Ciencias Exactas, Universidad Nacional de La Plata and Institute IFLP (CONICET), C. C. 67, (1900) La Plata, Argentina.*

‡ *Present address: Laboratoire de Spectrochimie Infrarouge et Raman, UMR CNRS 8516, Universite de Lille 1 Sciences et Technologies, Bat. C5, 59655 Villeneuve d'Ascq Cedex, France.*

† Electronic Supplementary Information (ESI) available: Tables of crystal data and structure refinement results (Table S1), fractional coordinates and equivalent isotropic displacement parameters of the non-H atoms (Tables S2), bond distances and angles (Table S3), atomic anisotropic displacement parameters (Tables S4), hydrogen atoms positions (Tables S5), and torsion angles (Table S6). ^{1}H and ^{13}C NMR data (Tables S7 and S8 and Figs. S1 and S2). Mass spectra (Table S9 and S10 and Fig. S3). Calculated energy minima (Tables S11 and S12 and Figs. S4 and S5). Calculated dipole moments and net atomic charges obtained by Mulliken population analysis (Table S13). Experimental and

theoretical IR and Raman wavenumbers (Tables S14 and S15). Wavelength and oscillator strength of the monoelectronic transitions (Tables S16 and S17) and theoretical electronic spectra (Figs. S6 and S7). Crystallographic structural data have been deposited at the Cambridge Crystallographic Data Centre (CCDC). Any request to the CCDC for this material should quote the full literature citation and the reference number CCDC 986379. See DOI: 10.1039/b000000x/

1 W. C. Zeise, *Tidsskrift for Naturvidenskaberne*, 1824, **I**, 82.
2 L. Jamir, R. Yella and B. K. Patel, *J. Sulfur Chem.*, 2009, **30**, 128.
3 A. Cambron and G. S Whitby, *Can. J. Res.*, 1930, **2**:(2) 144.
4 G. Losse and E. Wottgen, *J. Prak. Chem.*, 1961, **13**, 260.
5 M. H. Jones and J. T. Woodcock, *Anal. Chim. Acta* ,1987, **193**, 41.
6 A. M. Benson and P. B. Barretto, *Cancer Res.*, 1985, **45**, 4219.
7 L. W. Wattenberg, *Cancer Res.*, 1978, **26**, 197.
8 A. M. Benson, M. J. Hunkeler and J. L. York, *Biochem. J.*, 1989, **261**, 1023.
9 H. Haxthausen, *Acta Derm. Venereol.*, 1942, **22**, 346.
10 A. Björnberg and B. Friis, *Int J Dermatol.*, 1978, **17**, 69.
11 R. Felumb and B. Heilsen, *Acta Derm. Venereol*., 1952, **32**, S29, 95.
12 F. Sauterey, P. Branlard and P. Poullet, Patent No. US 5357010 A 19941018. Application: US 1993-22836 19930225.
13 S. Z. Zard, *Angew. Chem., Int. Ed. Engl*. 1997, **36**, 672.
14 F. Bertrand, V. Pevere, B. Quiclet-Sire and S. Z. Zard, *Org. Lett*. 2001, **3**, 1069.
15 G. Yuankai, H. Junpo, L. Changxi, Z. Changming, S. Shijie and Y. Yuliang, *Macromolecules*, 2010, **43**, 4500.
16 P. K. Ackerman, G. H. Harris, R. R. Klimpel and F. F. Aplan, *Int. J. Miner. Process.*, 1987, **21**, 105.
17 V. E. Vigdergauz and S. A. Kondrat'ev, *J. Min. Sci*., 2009, **45**, 4, 399.
18 J. Leja, Surface Chemistry of Froth Flotation; Plenum Press: New York, 1983.
19 G. S. Whitby and H. Greenberg, *Trans. R. Soc. Can*., 1929, **23**, 21.
20 R. Felumb, *B. Soc. Chim. Fr*., 1957, 890.
21 M. L. Shankaranarayana and C. C. Patel, *Can. J. Chem*., 1961, **39**, 1633.
22 V. F. Plyusnin, Y. V. Ivanov, V. P. Grivin, D.Y. Vorobjev, S. V. Larionov, A. M. Maksimov, V. E. Platonov, N. V. Tkachenko and H. Lemmetyinen, *Chem. Phys. Lett*., 2000, **325**, 153.
23 M. L. Shankaranarayana and C. C. Patel, *Spectrochim. Acta*, 1965, **21**, 95.
24 K. R. Bhaskar, *Ind. J. Chem.*, 1967, **5**, 416.
25 A. C. Larsson and S. Oberg, *J. Phys. Chem. A*, 2011, **115**, 1396.
26 G. N. Andreev and A. Barzev, *J. Mol. Struct*., 2003, **661-662**, 325.
27 C. C. DeWitt and E. E. Roper, *J. Am. Chem. Soc.*, 1932, **54**, 2, 444.
28 CAD4 Express Software. Enraf-Nonius, Delft, The Netherlands, 1994.
29 K. Harms and S. Wocadlo, XCAD4-CAD4 Data Reduction, University of Marburg, Marburg, Germany, 1995.
30 PLATON, A Multipurpose Crystallographic Tool, Utrecht University, Utrecht, The Netherlands, A. L. Spek, 1998.
31 G. M. Sheldrick, *Acta Crystallogr. Sec. A*, 2008, **A64**, 112.
32 M. J. Frisch, G. W. Trucks, H. B. Schlegel, G. E. Scuseria, M. A. Robb, J. R. Cheeseman, J. A. Montgomery, Jr., T. Vreven, K. N. Kudin, J. C. Burant, J. M. Millam, S. S. Iyengar, J. Tomasi, V. Barone, B. Mennucci, M. Cossi, G. Scalmani, N. Rega, G. A. Petersson, H. Nakatsuji, M. Hada, M. Ehara, K. Toyota, R. Fukuda, J. Hasegawa, M. Ishida, T. Nakajima, Y. Honda, O. Kitao, H. Nakai, M. Klene, X. Li, J. E. Knox, H. P. Hratchian, J. B. Cross, C. Adamo, J. Jaramillo, R. Gomperts, R. E. Stratmann, O. Yazyev, A. J. Austin, R. Cammi, C. Pomelli, J. W. Ochterski, P. Y. Ayala, K. Morokuma, G. A. Voth, P. Salvador, J. J. Dannenberg, V. G. Zakrzewski, S. Dapprich, A. D. Daniels, M. C. Strain, O. Farkas, D. K. Malick, A. D. Rabuck, K. Raghavachari, J. B. Foresman, J. V. Ortiz, Q. Cui, A. G. Baboul, S. Clifford, J. Cioslowski, B. B. Stefanov, G. Liu, A. Liashenko, P. Piskorz, I. Komaromi, R. L. Martin, D. J. Fox, T. Keith, M. A. Al-Laham, C. Y. Peng, A. Nanayakkara, M. Challacombe, P. M. W. Gill, B. Johnson, W. Chen, M. W. Wong, C. Gonzalez, and J. A. Pople, Gaussian 03, Revision B.01, Gaussian, Inc., Pittsburgh PA, 2003.
33 R. Bauernschmitt and R. Ahlrichs, *Chem. Phys. Lett.*, **256** (1996) 454.
34 R. E. Stratmann, G. E. Scuseria, and M. J. Frisch, *J. Chem. Phys.*, **109** (1998) 8218.
35 Y. A. Tobón, R. M. Romano, E. Hey-Hawkins, R. Boese and C. O. Della Védova, *J. Phys. Org. Chem*., 2009, **22**, 815.
36 Y. A Tobón, E. E. Castellano, O. E. Piro, C. O. Della Védova and R. M. Romano, *J. Mol. Struct.*, 2009, **930**, 43.
37 A. Hermann, S. E. Ulic, C. O. Della Védova, H. Mack and H. Oberhammer, *J. Fluorine Chem*., 2001, **112**, 297.
38 L. J. Farrugia, ORTEP3 for Windows: *J. Appl. Crystallogr*., 1997, **30**, 565.
39 Y. Watanabe, *Acta Cryst*., 1971, **B27**, 644.
40 A. Bondi, *J. Phys. Chem*., 1964, **68**, 441.
41 Weinhold F. and Landis, C. R. in Valency and Bonding: A Natural Bond Orbital Donor-Acceptor Perspective; Cambridge University Press., 2005.
42 Weinhold F. and Landis C. R., Getting Started in Discovering Chemistry With Natural Bond Orbitals, 2012 by John Wiley & Sons, Inc., Hoboken, NJ, USA.
43 V. R. Thalladi and R. Boese, *New J. Chem*., 2000, **24**, 579.
44 M. Podsiadło, A. Olejniczak and A. Katrusiak, , *J. Phys. Chem. C*, 2013, **117**, 4759.